Vibrational theory for monatomic liquids

Duane C. Wallace, Sven Rudin, Giulia De Lorenzi-Venneri, and Travis Sjostrom
Theoretical Division, Los Alamos National Laboratory, Los Alamos, New Mexico 87545, USA

(Received 17 January 2019; published 20 March 2019)

The construction of the vibration-transit theory of liquid dynamics is being presented in three sequential research reports. The first is on the entire condensed-matter collection of N-atom potential energy valleys and identification of the random valleys as the liquid domain. The present (second) report defines the vibrational Hamiltonian and describes its application to statistical mechanics. The following is a brief list of the major topics treated here. The vibrational Hamiltonian is universal, in that its potential energy is a single $3N$-dimensional harmonic valley. The anharmonic contribution is also treated. The Hamiltonian is calibrated from first-principles calculations of the structural potential and the vibrational frequencies and eigenvectors. Exact quantum-statistical-mechanical functions are expressed in universal equations and are evaluated exactly from vibrational data. Exact classical-statistical-mechanical functions are also expressed in universal equations and are evaluated exactly from a few moments of the vibrational frequency distribution. The complete condensed-matter distributions of these moments are graphically displayed, and their use in statistical mechanics is clarified. The third report will present transit theory, which treats the motion of atoms between the N-atom potential energy valleys.

DOI: 10.1103/PhysRevB.99.104204

I. INTRODUCTION

Vibration-transit (V-T) theory is about liquid dynamics, the motion of atoms in the liquid state, and primarily monatomic liquids at this time. The major theoretical development reached completion in a tractable description of the atomic motion, consisting of $3N$-dimensional normal-mode vibrations within a liquid potential energy valley, plus transits, in which the atoms move across the intervalley intersections. The vibrational theory is formally reduced to that of a single representative liquid valley and is presented in Sec. 23 of [1]. The transit theory was completed with the assignment to transits of a constant-volume measure of the melting entropy [2,3]. The corresponding theoretical equations for the thermodynamic functions were shown to provide an accurate account of experimental data for several elemental liquids [4,5].

Since then, we have carried out two large-scale quench studies designed to quantitatively organize the entire collection of valleys that constitute the potential energy surface (PES) of a monatomic system. This broad study provides a clearer understanding of the liquid vibrational theory by seeing it as a part of the whole condensed-matter theory. The first quench analysis identifies the random and symmetric distributions and describes the role of the random structures in V-T theory [6]. The second quench analysis defines and calibrates vibrational motion theory in one (any) $3N$-dimensional potential energy valley and is reported here. We are also in the final stages of a significant upgrade in transit theory. That research will complete the formal V-T theory of liquid thermodynamics, and we shall then undertake a comparison of theory and experiment for elemental liquids.

The present study is about two aspects of a single theoretical construct: the potential energy surface and the atomic motion. We write in terms of either aspect, depending on what we are trying to say. In constructing a configuration integral, we think in terms of the PES. On the other hand, a transit is the motion of an atom across an intervalley intersection. Working with both aspects provides a more incisive physical picture.

In Sec. II, we define the V-T decomposition, whose key function is to produce a tractable vibrational Hamiltonian. First, the low-lying harmonic portion of a $3N$-dimensional liquid valley is extended to infinity in all dimensions. A potential energy correction is then added to the Hamiltonian to account for the intervalley intersections, or what is equivalent, to account for the atomic transit motion across the intersections. Although the transit correction is complicated, it is relatively small, so that the decomposition makes a viable theory of liquid dynamics.

In Sec. III, for specific application to equilibrium thermodynamics, the vibrational Hamiltonian is calibrated from the normal-mode vibrational frequencies ω_λ, $\lambda = 1, 2, \ldots, 3N$. For thermodynamics, the normal-mode eigenvectors are not needed, but they are always available for more intricate statistical-mechanical applications. For a given set of ω_λ, the formally exact character of quantum statistical mechanics is observed and discussed.

In Sec. IV, we derive the exact statistical-mechanical equations for vibrational contributions to internal energy and entropy, valid at temperatures T at or above the melting temperature T_m. These equations are in the form of exact classical statistical mechanics plus quantum corrections. The equations are calibrated by a few characteristic temperatures θ_n, related respectively to the nth moment of the ω_λ distribution. Distributions of the key θ_n for the complete collection of condensed-matter potential energy valleys are shown graphically and discussed.

In Sec. V A, a descriptive list of the major theoretical arguments of the paper is given. In Sec. V B, properties of V-T

theory possibly useful to the equation of state (EOS) program are discussed.

II. THE V-T DECOMPOSITION

It has long been considered that the condensed-matter PES for monatomic systems consists of a great many $3N$-dimensional intersecting potential energy valleys. From extensive analysis of experimental thermodynamic data for elemental liquids and crystals, we have constructed a detailed description of those potential energy valleys, summarized in [6]. The valleys are of two classes, random and symmetric. The random valley manifold overwhelmingly dominates the PES, and is the domain of the liquid phase. The random valleys are macroscopically equivalent; that is, they all have the same macroscopic statistical-mechanical properties, so that one such valley can be used for statistical-mechanical calculations. Finally, the random valleys are harmonic to good approximation. These properties, demonstrated for elemental liquids having a wide variety of bonding types (Sec. II of [6]), strongly suggest the following V-T decomposition of the liquid potential energy surface.

The V-T decomposition is the defining construct of V-T theory. A single representative random structure is chosen for the liquid structure, according to the discussion in Sec. IV of [6]. For small displacements of the atoms from equilibrium at the liquid structure, the potential energy is, by definition, positive definite harmonic. This surface is first calibrated, as we shall describe in Sec. III, and is then extended to infinity in all $3N$ directions. This extension is necessary in order to create a tractable Hamiltonian. This Hamiltonian will provide the dominant contribution to V-T theory of liquid dynamics.

Next, we add a correction to account for error in the vibrational Hamiltonian. Formally, this error consists of the actual liquid potential energy surface minus the single $3N$-dimensional harmonic valley. In terms of the atomic motion instead of the potential surface, the correction requires us to account for the transit motion, in which atoms move across the intervalley intersections. Either way, this is a very complicated problem. However, the correction is small compared to the vibrational contribution, so the V-T decomposition actually qualifies as a net favorable theoretical construction.

We can illustrate the preceding discussion with molecular dynamics (MD) data for our liquid-Na system at $N = 500$ and constant volume V. Mean potential energy is denoted $\Phi(T)$. The system has two potential contributions, the vibrational $\Phi_{\rm vib}(T)$, which is known, and the correction, which is attributed to transits and denoted $\Phi_{tr}(T)$. Their sum is the potential $\Phi_{VT}(T)$ of V-T theory. However, in order to calibrate the theory from MD, we write

$$\Phi_{\rm MD}(T) = \Phi_{\rm vib}(T) + \Phi_{tr}(T). \tag{1}$$

The MD and vibrational curves are graphed in Fig. 1. The vibrational contribution is $\frac{3}{2}k_BT$, and the transit contribution is obvious as the difference $\Phi_{\rm MD} - \Phi_{\rm vib}$, from Eq. (1). Figure 1 clearly shows that the magnitude of $\Phi_{tr}(T)$ is small compared to that of $\Phi_{\rm vib}(T)$, to high temperatures. Experimental entropy data for elemental liquids show the same behavior as the potential energy shows in Fig. 1 [2,3].

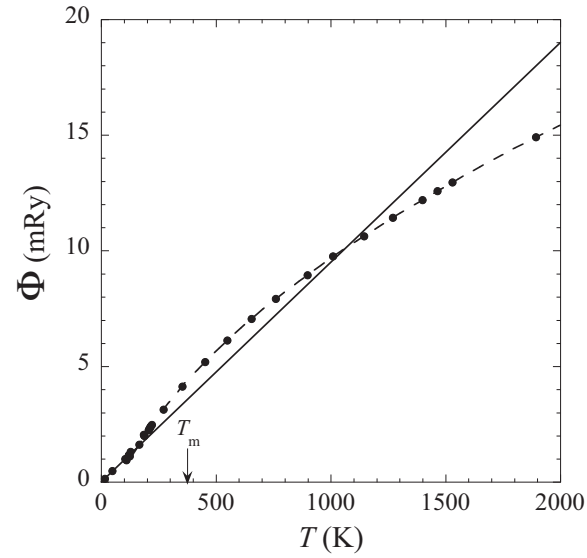

FIG. 1. The straight line is the vibrational potential energy $\Phi_{\rm vib} = \frac{3}{2}k_BT$, and dots fitted by the dashed line are total potential energy from MD $\Phi_{\rm MD}$. Φ_{tr} is $\Phi_{\rm MD} - \Phi_{\rm vib}$. The volume of the system is constant at $V_{lm} = 278a_0^3$, the volume of the liquid at melt. T_m is the temperature of the liquid at melt.

It is of interest to describe the physical character of the transit motion indicated in Fig. 1. First, notice that the actual MD potential energy at $T = 0$ is the liquid structure potential Φ_0^l. Here, however, Φ_0^l is set to zero since we are interested only in the thermal energy. As Fig. 1 shows, there are no transits up to around 150 K, but as T continues to increase, $\Phi_{tr}(T)$ increases from zero. This behavior correlates with the MD data for self-diffusion, which also measures zero up to T around 150 K, then increases from zero together with $\Phi_{tr}(T)$ (Fig. 10 of [7]). These MD calculations confirm that transits cause the diffusion.

With further increasing T, the continuing increase of $\Phi_{tr}(T)$ is mainly due to an increasing transit rate. The leveling of $\Phi_{tr}(T)$ results from a saturation of the liquid transits. The ultimate decrease of $\Phi_{tr}(T)$ is due to the removal of the vibrational potential energy surface at intervalley intersections. The latter effect, under the name of the "boundary effect," appears in the high-T, constant-V specific heat of elemental liquids and is exemplified by liquid Hg [8]. As T continues to increase in Fig. 1, $\Phi_{\rm MD}(T)$ falls increasingly below $\Phi_{\rm vib}(T)$ due to the increasing boundary effect, and the system embarks on a very broad liquid-to-gas transition (see, e.g., [9]).

III. CALIBRATION OF THE VIBRATIONAL HAMILTONIAN

To begin the vibrational calibration for a liquid, we carry out a number of quenches for the appropriate MD system and study several properties of the structures in order to identify the random structures [6]. We then choose a representative random structure for the liquid structure and calibrate the vibrational Hamiltonian as follows. The information contained in the liquid structure is its potential energy per atom Φ_0^l and the set $\{\mathbf{R}_{\rm K}\}$ of atomic equilibrium

positions for $K = 1, 2, \ldots, N$. The potential energy due to small displacements $\mathbf{u}_K$ of the atoms from equilibrium is a positive-definite quadratic form, i.e., a stable harmonic valley, in the $3N$ Cartesian components of the set $\{\mathbf{u}_K\}$. The matrix of potential energy coefficients, also called force constants, divided by the atomic mass M is the dynamical matrix. The eigenvalues of the dynamical matrix are ω_λ^2, where ω_λ is the vibrational frequency of mode λ, and $\omega_\lambda^2 > 0$ for $\lambda = 1, 2, \ldots, 3N-3$. The three translational modes having $\omega_\lambda = 0$ are removed for statistical-mechanical applications. As a matter of principle, the complete calibration must be done for a single structure.

The set of frequencies is all one needs to calculate vibrational contributions to the thermodynamic functions (see discussion of crystals on pp. 147–149 of [1]). However, the normal-mode eigenvectors are also valuable because they extend the coverage of vibrational statistical mechanics far beyond thermodynamics.

We generally make statistical-mechanical derivations in quantum formulation because that is the complete theory at all T. Classical expressions can be extracted from the quantum formulas, but the reverse is not possible. The formal theory of vibrational thermodynamics for any $3N$-dimensional harmonic valley is derived in Secs. 16 and 17 of [1], especially in Eqs. (16.13)–(16.20) and (17.1)–(17.8).

The normal vibrational modes obey Bose-Einstein statistics. The creation and annihilation operators are, respectively, A_λ^+ and A_λ for mode λ, and the vibrational Hamiltonian per atom is $\mathcal{H}_{\rm vib}$, where

$$\mathcal{H}_{\rm vib} = \frac{3}{3N-3}\sum_\lambda \hbar\omega_\lambda\left(A_\lambda^+ A_\lambda + \frac{1}{2}\right). \tag{2}$$

For mode λ, $\hbar\omega_\lambda$ is the vibrational-level spacing, $A_\lambda^+ A_\lambda$ measures the discrete occupation level in a system eigenfunction, and the term in $\frac{1}{2}$ is the zero-point energy. The mean occupation number is $n_\lambda(T) = \langle A_\lambda^+ A_\lambda\rangle$, where $\langle\cdots\rangle$ is the canonical average and

$$n_\lambda(T) = \frac{1}{e^{\beta\hbar\omega_\lambda}-1}, \quad \beta = \frac{1}{k_B T}. \tag{3}$$

The thermodynamic internal energy is $U_{\rm vib} = \langle\mathcal{H}_{\rm vib}\rangle$, so from Eq. (2),

$$U_{\rm vib}(T) = \frac{3}{3N-3}\sum_\lambda \hbar\,\omega_\lambda\left[n_\lambda(T) + \frac{1}{2}\right]. \tag{4}$$

The entire volume dependence of these equations is in $\omega_\lambda(V)$. These few equations are sufficient to illustrate the quantum formulation and to show in Sec. IV how we transform to the classical regime without losing information.

By derivation, a statistical-mechanical function is expressed as a sum over vibrational normal modes, e.g., $\sum_\lambda f_\lambda$ in Eq. (4), where f_λ expresses information belonging to mode λ. The information generally includes both frequency and eigenvector data. For thermodynamic functions, such a sum is traditionally replaced by an integral over the normalized frequency distribution $g(\omega)$ in the form $\int f(\omega)g(\omega)d\omega$, where $f(\omega)$ expresses information belonging to the increment $d\omega$ at ω. The integral formulation does not contain eigenvector information and therefore is limited to functions having no eigenvector dependence (see the discussion of Eq. (5.2) in [1]). The function $g(\omega)$ has become an investigative tool for comparing vibrational spectra of different systems.

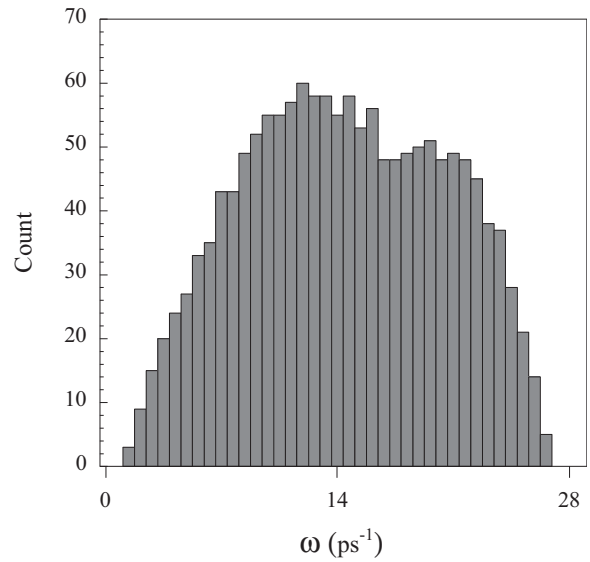

FIG. 2. Histogram of $g(\omega)$ from the set of vibrational frequencies ω_λ, calculated from the dynamical matrix. Calculations are based on the Na pair potential $\phi(r;V)$.

In Sec. IV, we shall test our Na calibration parameters by comparison with an independent density functional theory (DFT) calibration. We begin that comparison here. We work with histograms because that form introduces the minimal amount of extraneous information required to present the list of ω_λ in graphical form.

Figure 2 shows the liquid $g(\omega)$ as calculated from our Na potential, which has reliably produced excellent agreement with experimental data for crystal and liquid phases [1]. Figure 3 shows the liquid $g(\omega)$ computed from DFT. Both histograms display three characteristics commonly observed

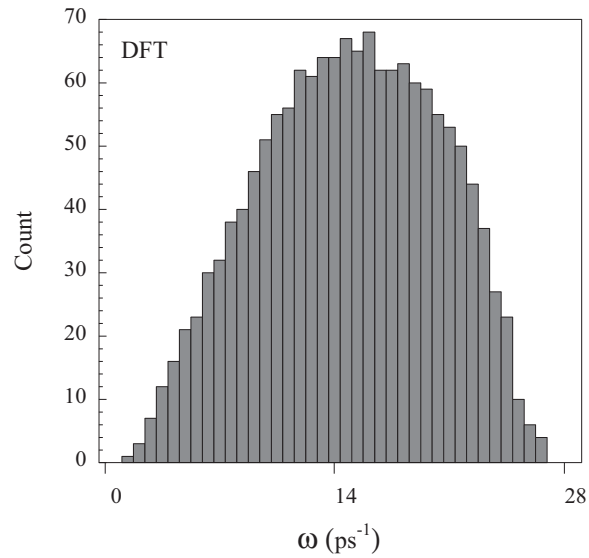

FIG. 3. Histogram of $g(\omega)$ made as in Fig. 2 from calculations based on first-principles DFT.

in our liquid studies to date: The low-ω edge is an accurate straight line that intersects zero count at $\omega > 0$; the high-ω edge is also a good straight line, steeper than the lower edge, and the top is roughly constant, with a two-step refinement that is pronounced in Fig. 2 and is weak in Fig. 3. From the overall similarity of the two graphs, we conclude that the fundamentally different computational methods will produce qualitatively similar vibrational thermodynamics for the liquid. A more incisive comparison appears at the end of Sec. IV.

IV. VIBRATIONAL STATISTICAL MECHANICS

Exact classical statistical mechanics is contained in the high-T expansion of quantum statistical mechanics. Under the high-T condition $(\hbar\omega_\lambda/k_BT) \ll 1$, Eq. (3) becomes

$$n_\lambda(T) + \frac{1}{2} = \frac{k_BT}{\hbar\omega_\lambda} \times \left[1 + \frac{1}{12}\left(\frac{\hbar\omega_\lambda}{k_BT}\right)^2 - \frac{1}{720}\left(\frac{\hbar\omega_\lambda}{k_BT}\right)^4 + \cdots\right]. \tag{5}$$

The first term on the right is classical theory, and the terms in $T^{-2}, T^{-4}, \ldots$ constitute the quantum correction series. By "classical regime" we mean temperatures at which the quantum correction is small but not necessarily negligible. We always keep at least the leading-order quantum correction because, as we shall see, it can provide an estimate of the entire series. Keeping the quantum correction also makes our calculated thermodynamic functions exact in principle in the classical regime.

From Eqs. (4) and (5), the vibrational internal energy per atom is

$$U_{\rm vib}(T) = \frac{3k_BT}{3N-3}\sum_\lambda \times \left[1 + \frac{1}{12}\left(\frac{\hbar\omega_\lambda}{k_BT}\right)^2 - \frac{1}{720}\left(\frac{\hbar\omega_\lambda}{k_BT}\right)^4 + \cdots\right]. \tag{6}$$

The sum $\sum_\lambda$ converts the numerators of the quantum correction terms into moments of the ω_λ distribution. Long ago, a set of *modified* moments of $g(\omega)$ was defined [10] and has since been widely applied (see, e.g., the compendium of crystal phonon data [11]). For application to lattice dynamics theory, we converted those moments to a set of characteristic temperatures θ_n, the natural dimension for scaling thermodynamics at high T (pp. 147–152 of [1]). These θ_n are now applied to liquid dynamics theory and are defined for $n \geqslant -3$ as follows:

$$k_B\theta_n = \left[\frac{n+3}{3}\frac{1}{3N-3}\sum_\lambda(\hbar\omega_\lambda)^n\right]^{1/n}, \quad n \neq 0 \text{ and } n \neq -3, \tag{7}$$

$$\ln(k_B\theta_0) = \frac{1}{3N-3}\sum_\lambda \ln(\hbar\omega_\lambda), \tag{8}$$

$$\theta_{-3} = \lim_{n\to-3}\theta_n. \tag{9}$$

Some technical notes are in order. First, the actual moments of [10], defined in terms of $g(\omega)$, are eliminated in the definitions (7)–(9). Equations (7)–(9) are in the exact statistical-mechanical formulation, as $\sum_\lambda f_\lambda$. Second, the scaling factor $(n+3)/3$ is present in all three equations (7)–(9). This scaling is not present in the standard definition of moments of a distribution but was inserted specifically to scale moments of a Debye distribution to a constant [10]. Simpler math would be to remove this spurious scaling, but it is by now a theoretical legacy.

To show the role of θ_n in vibrational thermodynamics, we list the equations for the internal energy and the entropy $S_{\rm vib}$:

$$U_{\rm vib}(V,T) = 3k_BT\left[1 + \frac{1}{20}\left(\frac{\theta_2(V)}{T}\right)^2 - \frac{1}{1680}\left(\frac{\theta_4(V)}{T}\right)^4 + \cdots\right], \tag{10}$$

$$S_{\rm vib}(V,T) = 3k_B\left[\ln\left(\frac{T}{\theta_0(V)}\right) + 1 + \frac{1}{40}\left(\frac{\theta_2(V)}{T}\right)^2 - \cdots\right]. \tag{11}$$

$F_{\rm vib}(V,T)$ is constructed from Eqs. (10) and (11) (see Eqs. (17.5)–(17.7) of [1]). For all such equations, θ_2 determines the first quantum correction. Higher terms can be estimated from $\theta_{2n} \approx \theta_2$, $n = 2, 3, \ldots$. θ_2 is also useful in the approximations $\theta_1 \approx \theta_2 \approx e^{\frac{1}{3}}\theta_0$ (p. 152 of [1]). Finally, $(k_B\theta_2)^2$ is proportional to the dynamical matrix trace, which can be evaluated without calculating the entire matrix (pp. 132–133 of [1]). Because θ_2 is easy to evaluate, it is often used as a general estimator for θ_n, $n \geqslant -2$. θ_0, Eq. (8), profoundly controls $S_{\rm vib}(V,T)$ by dominating its V dependence and scaling its T dependence in Eq. (11). The quantum zero-point vibrational energy is given by the term in $\frac{1}{2}$ in Eq. (4) and is expressed by the characteristic temperature θ_1 via the relation

$$\frac{3}{3N-3}\sum_\lambda \frac{1}{2}\hbar\omega_\lambda = \frac{9}{8}k_B\theta_1. \tag{12}$$

Hence, the liquid quantum ground-state energy is $\Phi_0^l + \frac{9}{8}k_B\theta_1$, while the classical ground-state energy is Φ_0^l. In the classical regime, the quantum zero-point energy disappears, and the high-T forms are pure classical plus small quantum corrections going as $T^{-2} + \cdots$.

θ_{-3} is the Debye temperature θ_D and has physical meaning only at very low temperatures. θ_D is theoretically given by sound velocities at $T = 0$, and θ_D scales the T dependence of specific heat at very low T (pp. 136, 162–165 of [1]).

For our well-studied Na MD system at $N = 500$, we carried out 1000 quenches to structures, calculated and diagonalized the dynamical matrix for each structure, and evaluated the sets of θ_n for $n = 2, 1, 0$. We refer to these as the central θ_n because these n measure most uniformly across the ω_λ distribution. θ_n for higher and lower n, respectively, concentrate on higher and lower ω_λ. The θ_n distributions are graphed against the distributions of the structural potential Φ_0 in Figs. 4–6. Each figure includes data points for 1 crystal and 18 symmetric and 982 random structures.

The dominant characteristic in Figs. 4–6 is the alignment of the entire θ_n distribution with the crystal-liquid axis for

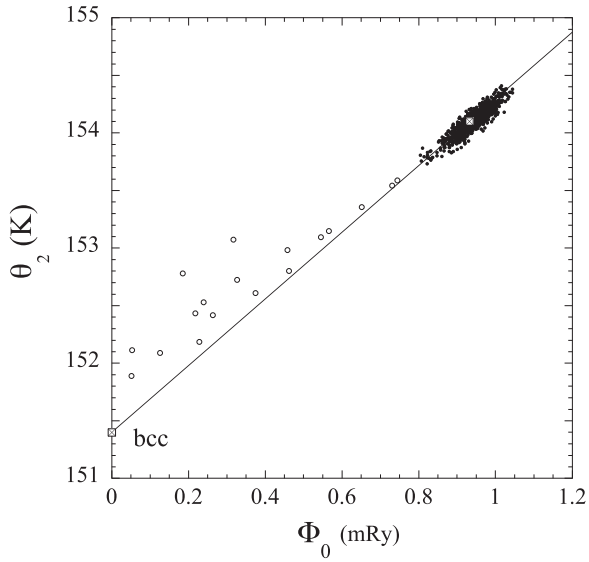

FIG. 4. Distribution of θ_2 from 1000 quenches to structures, graphed against the structure potential Φ_0. Solid dots are the random distribution, and the revealed cross indicates the liquid structure. Open circles are the symmetric distribution. The bcc crystal Φ_0 is set to zero for graphical clarity.

$n = 2$ and $n = 1$, with a small departure for $n = 0$. The slope of the axis decreases and passes through zero at n between 2 and 1 (Figs. 4 and 5). Where the slope is zero, $\theta_n^c = \theta_n^l$, and this is a qualitative measure of the most uniform weighting of ω_λ in Eq. (7) for $k_B\theta_n$. The largest scatter belongs to the symmetric distributions. That scatter is not random but shows a filamentary order that varies with n and signifies underlying structural symmetries. The graphs provide an organization of the entire condensed-matter distribution of central θ_n, and they invite us to investigate.

We shall now make specific application of Figs. 4–6 to the calibration of liquid vibrational theory. This will be done

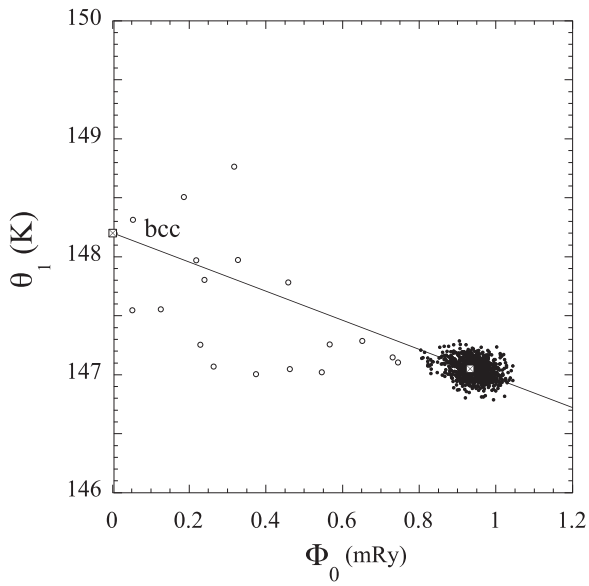

FIG. 5. Distribution of θ_1 (details are as in Fig. 4).

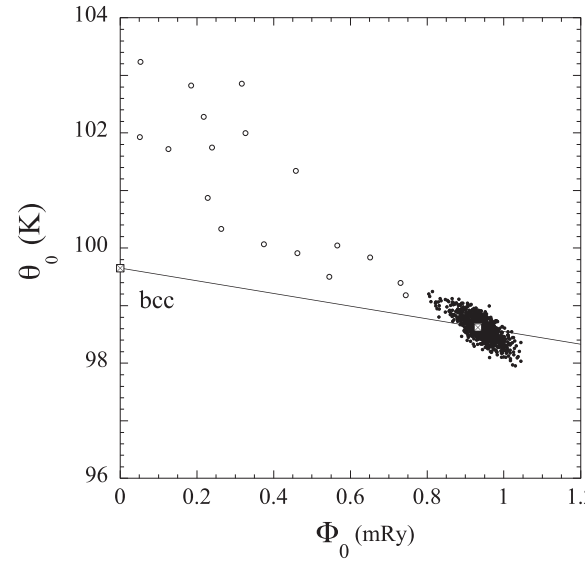

FIG. 6. Distribution of θ_0 (details are as in Fig. 4).

by making the same comparison here as in Sec. III for the same $g(\omega)$ shown in Figs. 2 and 3, but comparing the central θ_n instead of the $g(\omega)$ graphs. The θ_n are calculated directly from Eqs. (7) and (8), and they contain much more precise information than do the $g(\omega)$. The results are listed in Table I and discussed next.

Table I compares the central liquid θ_n^l between the Na potential calculation and the DFT calculation at the same volume V_{lm}. The deviation is defined as

$$\Delta\theta_n^l = \frac{\theta_n^l(\phi(r;V)) - \theta_n^l(\mathrm{DFT})}{\theta_n^l(\mathrm{DFT})}. \tag{13}$$

The deviation is systematic in n because the crystal-liquid axis changes with n. The deviation is sufficiently small that both computational methods are verified to high accuracy. We now have the capability to make first-principles calculations of the liquid vibrational parameters and hence of the liquid vibrational thermodynamics.

V. CONCLUSION

A. Theoretical concepts

Sections II–IV present a detailed description of the construction and calibration of the liquid vibrational theory. We shall now present a parallel description of the theoretical concepts that underlie the technical description. This presentation brings out the logic of V-T theory.

TABLE I. θ_n^l from the Na potential $\phi(r;V)$ is compared with θ_n^l from DFT. V is the volume per atom.

Data source	θ_2^l (K)	θ_1^l (K)	θ_0^l (K)	N	$V(a_0^3)$
$\phi(r;V)$	154.1	147.1	98.6	500	278
DFT	148.6	143.3	97.7	500	278
$\Delta\theta_n^l$	0.037	0.027	0.009		

(1) Of the vast number of potential energy valleys that constitute the condensed-matter PES, the random valleys are macroscopically equivalent and constitute the domain of the liquid phase. These concepts profoundly shape V-T theory. Vibrational theory is to be based on a single representative random valley, while a complex space of intervalley intersections becomes the research assignment.

(2) The philosophy of many-body theory guides us to the V-T decomposition in Sec. II. The motivation is to first construct a tractable Hamiltonian, which is done by extending the harmonic liquid valley to infinity. The tractable $\mathcal{H}_{\rm vib}$ is written in Eq. (2). The equally important companion step is to show that the Hamiltonian correction required to achieve liquid behavior is relatively small, which is done in Fig. 1. These two steps alone qualify the formulation as an acceptable starting point for a liquid dynamics theory.

(3) Vibrational calibration parameters are evaluated at a liquid structure. For logical clarity, we keep the structural potential Φ_0^l separate from the atomic motion. The vibrational parameters are then the equilibrium positions $\{\mathbf{R}_{\rm K}\}$, the mode frequencies $\{\omega_\lambda\}$, and the mode eigenvectors. These parameters measure a representative potential energy valley belonging to the liquid domain of the PES. In other words, the calibration measures the potential surface that drives the liquid atomic motion. This is the correct physical calibration.

(4) Given the quantum Hamiltonian, Eq. (2), statistical-mechanical equations are derived by analysis and are formally exact. These equations are expressed as sums over eigenmodes λ. Equations (2)–(12) of the present study are formally exact. They are subject to zero theoretical error, by definition, and are subject only to numerical error, which includes finite-N error. We avoid the integral formulation of thermodynamics (Sec. II), as it can express only a small segment of statistical mechanics theory.

(5) The high-T expansion of quantum statistical mechanics is useful because it separates into exact classical statistical mechanics plus the quantum correction, Eqs. (7)–(12). The classical theory is easy to work with because its liquid thermodynamics is primarily calibrated by just three parameters, the central θ_n, and the quantum correction goes to zero as T increases above T_m.

(6) The deviations between the liquid central θ_n^l from two different computational methods are listed in Table I. These deviations serve as an estimate of error in the vibrational calibration for monatomic liquids. The consequent relative error in the functions $U_{\rm vib}(T)$ and $S_{\rm vib}(T)$ is on the order of 0.005 at T_m and decreases as T increases from T_m. We conclude that the liquid vibrational thermodynamics can, in practice, be evaluated to negligible error.

B. Relations of V-T theory to EOS modeling

Modeling of the thermodynamic properties of the liquid state has a long history with extensive literature, beginning with van der Waals's famous two-term equation [12] and going to contemporary research, which may involve hundreds of terms and parameters [13]. Improved accuracy in the measurements of the thermodynamic properties has led to the continuing development and complexities of the EOS models [14–16]. Those complex EOSs are capable of accuracy within a fraction of a percent of the experimentally measured values. In a more general scope, beyond just fluids, a standard three-term free-energy construction of the EOS is often used [17–19] with accuracies of a few percent. The first contribution of the EOS construction is that of the zero-temperature compression response curve, which in V-T theory is the liquid ground-state energy [6]. The second EOS model contribution is the thermal response related to the atomic motion, which in V-T theory has vibrational contributions discussed in this paper plus a transit contribution. Finally, the third EOS term is that related to the electronic thermal excitation with temperature, and V-T theory contains the same term. While these EOSs are constructed as a single phase, V-T theory is developed within the multiphase EOS program and represents the liquid. The vibrational contribution is first principles and can be evaluated at any volume.

The general EOS liquid models often treat the thermal atomic response as being Debye-like near melt, which is experimentally motivated for metallic systems [20], and then interpolate to the extremely high temperature ideal-gas limit [21]. This interpolation is constrained by shock Hugoniot data into the liquid regime and increasingly by *ab initio* simulation [22,23]. Increases in the quantity and accuracy of the constraining data have shown deficiencies in these interpolative models [24], which leads to the same path of needing more parameters in increasingly complex models to cover the regimes of interest. In order to extend our formulation beyond V-T theory, to the ideal gas, we are developing an appropriate tractable Hamiltonian to replace the numerical interpolation.

Over many years of development, liquid dynamics theory has included consideration of many-atom correlated vibrational motion, referred to as "collective modes," or "phonons." In an exemplary study early in the development of collective motion theory, the liquid dynamics was represented by a set of propagating periodic density fluctuations in the form of Fourier transforms of the atomic positions and momenta [25]. The theoretical objective was to modify the transforms to make the atomic motion consistent with a Hamiltonian based on interatomic central potentials. This part of the approach did not survive. Later, longitudinal and transverse phonons in metallic liquids were described in detail (Secs. 3.14 and 3.15 in [26]). In the spirit of inquiry, Fourier components of the density operator were treated as phonons (Secs. 8.5 and 8.6 of [27]). In the "phonon theory of liquid dynamics," thermodynamic functions are formulated in terms of a Debye distribution of vibrational modes plus a modification of the lowest-frequency transverse modes to account for diffusive motion [28–32]. The modification is calibrated from the viscosity relaxation time, which is T dependent. Experimental data have been employed to test and develop the theory for a wide variety of liquid types and wide ranges of V and T [29,33–35]. These references also provide a thorough compilation of published data supporting the presence of collective modes in liquid dynamics.

In V-T theory, as described in Secs. II–IV, liquid vibrational motion is attributed to the actual quantum vibrational modes, as calculated from the actual liquid potential energy surface. For the necessary companion component of liquid atomic motion, we shall turn next to a detailed presentation of transit theory.

ACKNOWLEDGMENTS

We would like to thank B. Clements for helpful and encouraging discussions. This work was supported by the U.S. Department of Energy through the Los Alamos National Laboratory. Los Alamos National Laboratory is operated by Triad National Security, LLC, for the National Nuclear Security Administration of the U.S. Department of Energy (Contract No. 89233218CNA000001).

[1] D. C. Wallace, *Statistical Physics of Crystals and Liquids* (World Scientific, River Edge, NJ, 2002).
[2] D. C. Wallace, E. D. Chisolm, and N. Bock, Phys. Rev. E **79**, 051201 (2009).
[3] D. C. Wallace, E. D. Chisolm, N. Bock, and G. De Lorenzi-Venneri, Phys. Rev. E **81**, 041201 (2010).
[4] N. Bock, E. Holmström, T. B. Peery, R. Lizárraga, E. D. Chisolm, G. De Lorenzi-Venneri, and D. C. Wallace, Phys. Rev. B **82**, 144101 (2010).
[5] S. P. Rudin, N. Bock, and D. C. Wallace, Phys. Rev. B **90**, 174109 (2014).
[6] T. Sjostrom, G. De Lorenzi-Venneri, and D. C. Wallace, Phys. Rev. B **98**, 054201 (2018).
[7] D. C. Wallace and B. E. Clements, Phys. Rev. E **59**, 2942 (1999).
[8] D. C. Wallace, Phys. Rev. E **57**, 1717 (1998).
[9] D. C. Wallace, B. L. Holian, J. D. Johnson, and G. K. Straub, Phys. Rev. A **26**, 2882 (1982).
[10] T. Barron, W. Berg, and J. Morrison, Proc. R. Soc. London, Ser. A **242**, 478 (1957).
[11] H. Schober and P. Dederichs, in *Phonon States of Elements. Electron States and Fermi Surfaces of Alloys*, edited by K.-H. Hellwege, Landolt-Börnstein - Group III Condensed Matter Vol. 13a (Springer, Berlin, 1981).
[12] J. D. Van der Waals, Ph.D. thesis, University of Leiden, 1873 .
[13] L. V. Woodcock, Entropy **20**, 22 (2018).
[14] R. Span and W. Wagner, J. Phys. Chem. Ref. Data **25**, 1509 (1996).
[15] B. Schmid and J. Gmehling, J. Supercrit. Fluids **55**, 438 (2010).
[16] J. S. Lopez-Echeverry, S. Reif-Acherman, and E. Araujo-Lopez, Fluid Phase Equilib. **447**, 39 (2017).
[17] S. P. Lyon and J. D. Johnson, Los Alamos National Laboratory, Technical Report No. LA-UR-92-3407, 1992.
[18] V. N. Zharkov, *Equations of State for Solids at High Pressures and Temperatures* (Springer, New York, 1971).
[19] O. Anderson, *Equations of State for Solids in Geophysics and Ceramic Science* (Oxford University Press, New York, 1995).
[20] J. R. D. Copley and J. M. Rowe, Phys. Rev. Lett. **32**, 49 (1974).
[21] J. D. Johnson, High Pressure Res. **6**, 277 (1991).
[22] T. Sjostrom, S. Crockett, and S. Rudin, Phys. Rev. B **94**, 144101 (2016).
[23] T. Sjostrom and S. Crockett, Phys. Rev. E **97**, 053209 (2018).
[24] S. C. Burnett, D. G. Sheppard, K. G. Honnell, and T. Sjostrom, in *Shock Compression of Condensed Matter - 2017: Proceedings of the Conference of the American Physical Society Topical Group on Shock Compression of Condensed Matter*, edited by R. Chau, T. C. Germann, J. M. D. Lane, E. N. Brown, J. H. Eggert, and M. D. Knudson, AIP Conf. Proc. No. 1979 (AIP, New York, 2018), p. 030001.
[25] R. Eisenschitz and M. J. Wilford, Proc. Phys. Soc. **80**, 1078 (1962).
[26] T. E. Faber, *Introduction to the Theory of Liquid Metals* (Cambridge University Press, New York, 1972), Chaps. 3.14 and 3.15.
[27] N. H. March, *Liquid Metals: Concepts and Theory* (Cambridge University Press, New York, 1990), Chaps. 8.5 and 8.6.
[28] Y. D. Fomin, V. N. Ryzhov, E. N. Tsiok, J. E. Proctor, C. Prescher, V. B. Prakapenka, K. Trachenko, and V. V. Brazhkin, J. Phys.: Condens. Matter **30**, 134003 (2018).
[29] K. Trachenko and V. V. Brazhkin, Rep. Progr. Phys. **79**, 016502 (2016).
[30] K. Trachenko and V. V. Brazhkin, Ann. Phys. (N.Y.) **347**, 92 (2014).
[31] K. Trachenko, Phys. Rev. B **78**, 104201 (2008).
[32] C. Yang, M. T. Dove, V. V. Brazhkin, and K. Trachenko, Phys. Rev. Lett. **118**, 215502 (2017).
[33] D. Bolmatov, V. V. Brazhkin, and K. Trachenko, Sci. Rep. **2**, 421 (2012).
[34] D. Bolmatov and K. Trachenko, Phys. Rev. B **84**, 054106 (2011).
[35] V. V. Brazhkin, Y. D. Fomin, A. G. Lyapin, V. N. Ryzhov, and K. Trachenko, Phys. Rev. E **85**, 031203 (2012).